DOI 10.1007/s11106-021-00238-w
Powder Metallurgy and Metal Ceramics, Vol. 60, Nos. 5-6, September, 2021 (Russian Original Vol. 60, Nos. 5-6, May-June, 2021)

THEORY AND TECHNOLOGY OF SINTERING, THERMAL AND THERMOCHEMICAL TREATMENT

THE DENSIFICATION KINETICS OF POROUS ZIRCONIUM DIBORIDE IN VACUUM PRESSURE SINTERING

M.S. Kovalchenko,[1,2] V.B. Vinokurov,[1] R.V. Litvin,[1] and L.I. Klimenko[1]

UDC 536.97:546.831'271:621.762.4/.5

The time dependence of densification for a zirconium diboride powder during the isothermal sintering in vacuum assisted with applied pressure varying from 12 to 60 MPa in the range 2110–2300°C and the nonisothermal pressure sintering with temperature being constantly increased by 20 and 40°C/min was studied experimentally. The densification kinetics was analyzed within the framework of continuum theory for bulk viscous flow taking the powder particle shape influenced the rheological properties of porous bodies into account. The densification kinetics was represented by equations describing nonlinear steady-state creep of the matrix forming a porous body. In isothermal sintering conditions, the root-mean-square strain rate is proportional to the fourth exponent of the root-mean-square stress. The creep is controlled by the dislocation climb mechanism with an estimated activation energy that is equal to 626 kJ/mol and is consistent with the activation energy for self-diffusion of atoms in the metal sublattice of borides. The estimated Laplace pressure is virtually comparable with the average applied pressure. The root-mean-square shear stress induced by additive pressure decreases with increase in the relative density and approaches zero at near-theoretical density of the material. The root-mean-square strain rate sharply decreases in the isothermal sintering process and increases reaching the maximum on the nonisothermal sintering curve. Two temperature ranges with different activation energies were found for nonisothermal pressure sintering. The higher temperature range is characterized by energies that are significantly greater than those for isothermal sintering and is indicative of endothermic process. The estimated critical cold brittleness temperature for zirconium diboride to transform to plastic condition is 1345°C.

Keywords: *porous zirconium diboride, pressure sintering, nonisothermal sintering, densification kinetics, activation energy, cold brittleness.*

[1]Frantsevich Institute for Problems of Materials Science, National Academy of Sciences of Ukraine, Kyiv, Ukraine.

[2]To whom correspondence should be addressed; e-mail: mikkov@ukr.net.

Translated from Poroshkova Metallurgiya, Vol. 60, Nos. 5–6 (539), pp. 25–41, 2021. Original article submitted April 16, 2021.

INTRODUCTION

The densification kinetics of powders in the sintering process should be understood well to determine the optimal conditions for imparting the desired structure and properties to materials produced from refractory compounds employing powder metallurgy techniques. Zirconium diboride composites [1–8] deserve special attention among the materials in this class as they retain adequate strength up to higher temperatures than other similar materials do. The addition of densification activating impurities intensifies the process, reduces the residual porosity, and increases the mechanical properties at low and medium temperatures [9], while slightly lowering the upper-temperature threshold of the material application.

Therefore, in present work the kinetics of zirconium diboride densification during the pressure sintering in vacuum at different temperature modes was investigated.

We first intended to carry out a narrow study of nonisothermal sintering kinetics, which would involve a limited scope of isothermal sintering experiments with pressure being varied at one chosen temperature, required to estimate the Laplace pressure using data from analysis of the densification kinetics. However, a preliminary analysis of nonisothermal pressure sintering kinetics revealed unexpectedly high activation energies and thus prompted us to carry out isothermal pressure sintering with temperature being varied from 2100 to 2300°C and pressure from 12 to 60 MPa.

STARTING MATERIALS AND EXPERIMENTAL PROCEDURE

The as-delivered ZrB_2 powder (H.C. Stark Company) with an average particle size of 2 μm was used for the experiments. The powder contained admixtures (wt.%) such as 0.2 Hf, 0.08 C, 0.09 Fe, 0.78 O, and 0.1–0.13 B_2O_3.

A laboratory high-temperature press machine with a 0.05 m^3 vacuum chamber [10] was employed for pressure sintering. A device was mounted inside the press for resistive heating of molds with a low-voltage (within 8 V) current from the grid through power and variable-output standard transformers. The shrinkage was monitored with a dilatometer. The press machine was equipped with a system of levers and weights to maintain the preset pressure, which can hardly be reached in hydraulic presses. Molds made of MPG-7 graphite, 120 mm high with an outer diameter of 26 mm and an inner diameter of 8 mm, were used for sintering. The die inner walls of mold were preliminary covered with a thin boron nitride layer as a high-temperature lubricant. To prevent the influence of size factors, the powder to be densified had the weight determined to produce compact sintered samples 10 ± 0.5 mm in height.

Pressure was applied before the heating. The heating rate at preset temperatures was 1500–2000°C/min. The sintering temperature was monitored with a Termix K infrared thermometer with an error of ±1%. Changes in the height of the sample were recorded with a linear displacement sensor with an accuracy of 0.01 mm. The current values of temperature and linear shrinkage were recorded automatically every five seconds.

The current values of linear shrinkage x_i and final relative density and height h_f of the samples were used to determine the current values of relative density:

$$\rho = \frac{\gamma_f h_f}{(h_0 - x_i)\gamma_{th}}, \quad (1)$$

where $h_0 = h_f + x_f$ is the initial height and γ_{th} is the theoretical density [11].

The densification kinetics was analyzed quantitatively within the framework of continuum theory for bulk viscous flow of porous bodies [12–15]. The theory relies on the fundamental feature of a viscous porous body that deforms as a composite with pores that have no material properties. In the case of irreversible deformation, this means that the total dissipation (scattering) of energy throughout a porous body is the same as the dissipation of energy in a material matrix formed by an ensemble of powder particles. Considering the scientific principle of irreversibility resulting from energy dissipation and applying the hydrodynamic analogy of the elasticity theory for highly viscous bodies and appropriate mathematical tools, relationships to determine the root-mean square stress

$\langle\tau_m\rangle$ and strain rate $\langle\dot{\varepsilon}_m\rangle$ in the porous body matrix were derived in the above papers from the current relative density ρ, densification rate $(d/dt)\rho$, and total pressure acting on the porous body in a mold:

$$\langle\tau_m\rangle = P\sqrt{\frac{1-2\nu}{\rho\varphi(1-\nu)}} = P\sqrt{\frac{2\left(1-\rho^{(1+\rho)/\rho}\right)}{\rho^{2.5/\rho}\left(2-\rho^{(1+\rho)/\rho}\right)}}\ ; \tag{2}$$

$$\langle\dot{\varepsilon}_m\rangle = \frac{1}{\rho}\frac{d\rho}{dt}\sqrt{\frac{1}{\rho}\left(\psi+\frac{2}{3}\varphi\right)} = \frac{1}{\rho}\frac{d\rho}{dt}\rho^{(2.5-2\rho)/(2\rho)}\sqrt{\frac{2-\rho^{(1+\rho)/\rho}}{2\left(1-\rho^{(1+\rho)/\rho}\right)}}\ . \tag{3}$$

Here P is the axial pressure; $\nu = \nu_m\rho^{(1+\rho)/\rho}$ (exponent 2/ρ was corrected to (1 + ρ)/ρ upon analysis of recent efforts on the densification of powders with low initial relative density); and ν_m is Poisson's ratio of the porous body matrix ($\nu_m = 1/2$ for viscous and plastic bodies). The φ and ψ values for powder materials formed by regular near-spherical powder particles [16] were found as follows:

$$\varphi = \rho^{(2.5-\rho)/\rho};\ \psi = \frac{1}{3}\varphi\frac{1+\nu}{1-2\nu} = \frac{1}{6}\rho^{(2.5-\rho)/\rho}\frac{2+\rho^{(1+\rho)/\rho}}{1-\rho^{(1+\rho)/\rho}}\ . \tag{4}$$

For powder materials formed by irregular particles, $\varphi = \rho^{(3.5-\rho)/\rho}$.

At high sintering temperatures, the viscous flow of the porous body matrix is controlled by the mechanism of nonlinear steady-state creep of a porous crystalline body described as

$$\langle\dot{\varepsilon}_m\rangle = \frac{1}{2}A\left(\frac{\langle\tau_m\rangle}{\tau_{m(0)}}\right)^n, \tag{5}$$

where n is the nonlinearity exponent for viscous flow;

$$A = \text{const}\frac{D_0\mu_m b}{k_B T}\exp\left(-\frac{U}{k_B T}\right), \tag{6}$$

where D_0 is the preexponential factor for the bulk self-diffusion coefficient; U is the activation energy; μ_m is the elastic shear modulus; b is the Burgers vector; T is the thermodynamic temperature; k_B is the Boltzmann constant; and $\tau_{m(0)}$ is the matrix yield stress [17].

The substitution of Eqs. (2) and (3) to Eq. (5) produces an equation describing the pressure sintering kinetics of a porous crystalline body in a mold:

$$\rho^{\frac{2.5(n+1)-4\rho}{2\rho}}\left(\frac{2-\rho^{(1+\rho)/\rho}}{2\left(1-\rho^{(1+\rho)/\rho}\right)}\right)^{\frac{n+1}{2}}\frac{d\rho}{dt} = \frac{1}{2}A\left(\frac{P}{\tau_{m(0)}}\right)^n = \frac{d}{dt}X_{d(2)}(n,\rho) = \dot{X}_{d(2)}(n,\rho); \tag{7a}$$

$$\rho^{\frac{3.5(n+1)-4\rho}{2\rho}}\left(\frac{2-\rho^{(1+\rho)/\rho}}{2\left(1-\rho^{(1+\rho)/\rho}\right)}\right)^{\frac{n+1}{2}}\frac{d\rho}{dt} = \frac{1}{2}A\left(\frac{P}{\tau_{m(0)}}\right)^n = \frac{d}{dt}X_{d(3)}(n,\rho) = \dot{X}_{d(3)}(n,\rho). \tag{7b}$$

The left terms of the equations are somewhat cumbersome, and their shorter versions are given on the right. The integration of the left and middle terms of the equations provides linear time dependences of the integral function for relative density:

$$X_{d(2)}(n,\rho) = \int_{\rho_0}^{\rho}\rho^{\frac{2.5(n+1)-4\rho}{2\rho}}\left(\frac{2-\rho^{(1+\rho)/\rho}}{2\left(1-\rho^{(1+\rho)/\rho}\right)}\right)^{\frac{n+1}{2}}d\rho = \frac{1}{2}A\left(\frac{P}{\tau_{m(0)}}\right)^n t\ ; \tag{8a}$$

$$\mathrm{X}_{\mathrm{d}(3)}(n,\rho)=\int_{\rho_0}^{\rho}\rho^{\frac{3.5(n+1)-4\rho}{2\rho}}\left(\frac{2-\rho^{(1+\rho)/\rho}}{2\left(1-\rho^{(1+\rho)/\rho}\right)}\right)^{\frac{n+1}{2}}\mathrm{d}\rho=\frac{1}{2}A\left(\frac{P}{\tau_{\mathrm{m}(0)}}\right)^{n}t\,, \tag{8b}$$

describing the densification kinetics of a porous body in isothermal pressure sintering controlled by the steady-state creep mechanism at constant A. The expressions under the integral signs combine time dependences of the root-mean-square strain rates and stresses and collectively express the pressure sintering behavior of a porous body. At $n = 1$, there is no $\tau_{\mathrm{m}(0)}$ in the viscous flow equation and, hence, it can be accepted as the threshold stress above which nonlinear flow occurs. If we fit Eqs. (7a) and (7b) to equation

$$\dot{\mathrm{X}}_{\mathrm{d}}(n,\rho)=\frac{1}{2}BP^{n}=\frac{P}{2\eta_{\mathrm{m}}} \tag{9}$$

(where η_{m} is the matrix viscosity), then fluidity $1/\eta_{\mathrm{m}}=BP^{n-1}$ becomes independent of $\tau_{\mathrm{m}(0)}$, which is important for estimating the activation energy with Eqs. (7a) and (7b) with substitution of A to them. Using the short form of the equations, the ratios of densification rates at temperatures T_1 and T_2 and constant P/τ_{m} are determined as

$$\frac{T_2\dot{\mathrm{X}}^{(2)}_{\mathrm{d}(2)}(n,\rho)}{T_1\dot{\mathrm{X}}^{(1)}_{\mathrm{d}(2)}(n,\rho)}=\exp\left\{\frac{U}{k_{\mathrm{B}}}\left(\frac{1}{T_1}-\frac{1}{T_2}\right)\right\}\,, \tag{10}$$

and a known equation to estimate the activation energy is obtained after taking logarithms and some algebra:

$$U=k_{\mathrm{B}}\frac{T_1T_2}{T_2-T_1}\left\{\ln\frac{T_2\dot{\mathrm{X}}^{(2)}_{\mathrm{d}(2)}(n,\rho)}{T_1\dot{\mathrm{X}}^{(1)}_{\mathrm{d}(2)}(n,\rho)}\right\}\,. \tag{11}$$

According to these equations, the activation energy at constant initial temperature T_0 is found from logarithmic dependences $\ln\left\{T\dot{\mathrm{X}}_{\mathrm{d}(2)}(n,\rho)\right\}$ and $\ln\left\{T\dot{\mathrm{X}}_{\mathrm{d}(3)}(n,\rho)\right\}$ vs. reciprocal thermodynamic temperature T^{-1}.

ISOTHERMAL PRESSURE SINTERING

Isothermal pressure sintering of porous materials, at least at a certain constant temperature and varied pressure, should be carried out in all conditions to estimate the Laplace pressure promoting the densification of a porous body in pressureless sintering. Zirconium diboride was first sintered under pressure by accelerated heating at a rate of 1500–2000°C/min to 2110°C and then held isothermally for 20–25 min. The data on variation in the height of samples found with Eq. (1) were used to determine the dependence of their relative density on sintering time at pressures of 12, 24, 36, 48, and 60 MPa. To confirm that the data are reliable, sintering was repeated three times in each mode.

Averaging and smoothing the shape of the relative density dependence curves and the rate of its change over time by the method of piecewise polynomial approximation by the least squares criterion did not always give satisfactory join of parts of the density curves, and especially the time dependence of densification rate curves. For this reason, we first calculated integral dependences (8a) and (8b) for each individual curve $\rho(t)$ with varying flow nonlinearity n using author's custom Fortran codes in order to determine the linearity and slope of the integrals to the time axis, which can be easily averaged in the case of straight lines. The integral dependences turned out to be upward curves at $n > 3$ and then tended to straighten after the first several minutes. Hence, time was counted from the moment the curve was becoming a straight line. The results indicate that the time dependences of the integral functions represented by Eqs. (8a) and (8b) become linear at $n = 4.5$ and $n = 4$, respectively. Figure 1 shows the integral function of relative density, $\mathrm{X}_{\mathrm{d}(3)}(n=4,\rho)$, versus time of pressure sintering in vacuum.

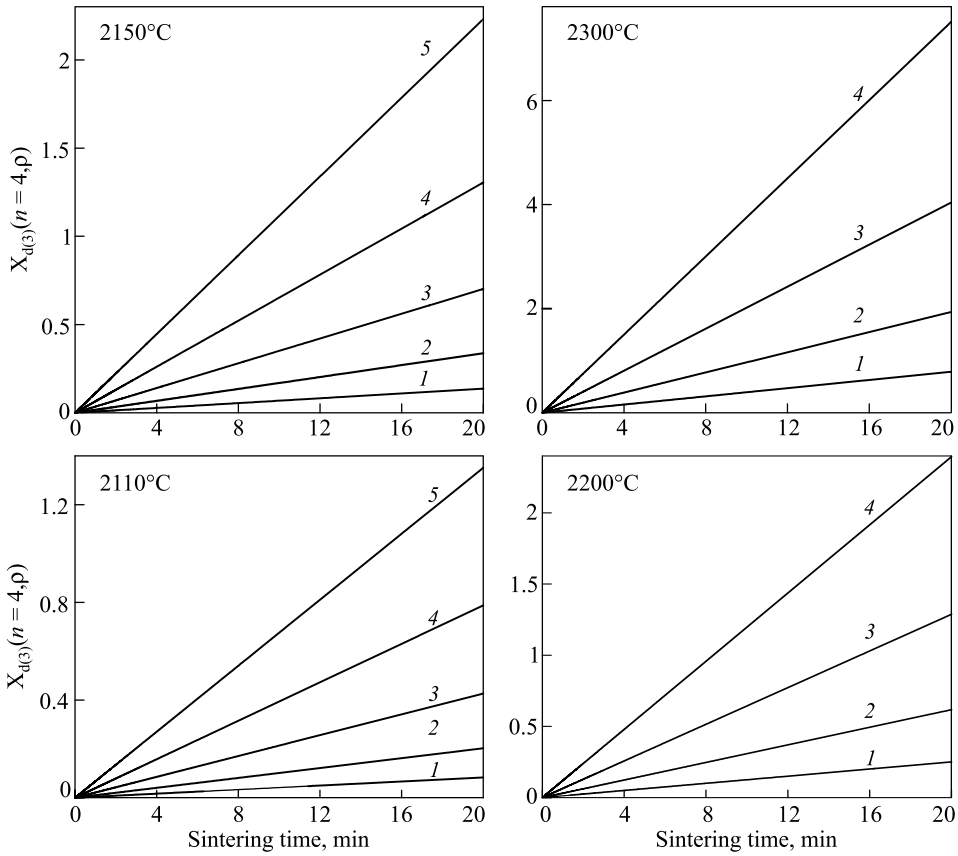

Fig. 1. Integral functions of relative density $X_{d(3)}(n=4,\rho)$ vs. pressure sintering time at 12 (*1*), 24 (*2*), 36 (*3*), 48 (*4*), and 60 MPa (*5*) in vacuum

The linearity of the averaged integral functions $X_{d(3)}(n=4,\rho)$ vs. the sintering time enables the solution of the inverse problem of calculating the averaged values of the current density of samples in the sintering process according to the average values of their initial and final density. To obtain a representative data set, programmable integration with a small step of relative density was carried out, recording the dependences of the current values of the integral function on the current values of its argument ρ. Since the integral functions are linearly dependent on time, the inversion of the obtained dependences in changing the scale of the dimensionless integral functions to the time scale gives inverse dependences of the relative density on time. The time dependences for the relative density of zirconium diboride during the pressure sintering in vacuum are shown in Fig. 2.

The slope β_X of line in Fig. 1 corresponds to the left-hand part of densification kinetics equation (7b), $\beta_X = X_{d(3)}(n=4,\rho)/t = \dot{X}_{d(3)}(n=4,\rho)$. The product $R\cdot(-\beta_X)$, where R = 8.31446261815 J/(mol · K) is the universal gas constant, gives the activation energy in J/mol. The slope of these lines under the same pressure and further calculation of the linear dependences $\ln\{T\dot{X}_{d(3)}(n=4,\rho)\}$ and $\ln\{T\dot{X}_{d(2)}(n=4.5,\rho)\}$ as a function of reciprocal temperature T^{-1} (Fig. 3) enables the estimation of the activation energy of the creep mechanism controlling the densification kinetics during the pressure sintering of porous bodies. The estimated activation energies are 655 kJ/mol for $\ln\{T\dot{X}_{d(2)}(n=4.5,\rho)\}$ and 626 kJ/mol for $\ln\{T\dot{X}_{d(3)}(n=4,\rho)\}$. They are typical for the self-diffusion activation energy in metal sublattice of refractory carbides and borides and indicate that the densification kinetics in high-temperature pressure sintering is controlled by the dislocation climb mechanism.

In the general case, the densification kinetics nonlinearly depends on pressure; hence, the *n*-th roots are to be taken for both parts of kinetic equations (7) to transform them into linear dependences. This transformation for the sintering of ZrB_2 at 2110°C is shown in Fig. 4. The initial sections of the kinetic lines do not start at the origin

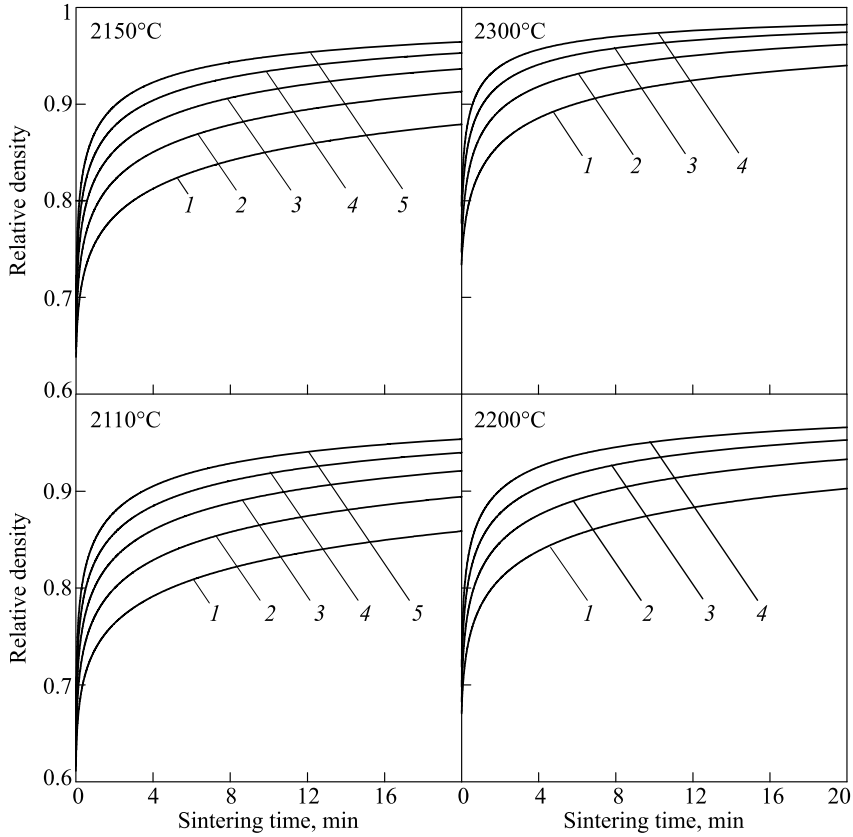

Fig. 2. Relative density of porous ZrB_2 vs. isothermal sintering time at an applied pressure of 12 (*1*), 24 (*2*), 36 (*3*), 48 (*4*), and 60 MPa (*5*) in vacuum

but lie on the pressure axis far to the left of the origin and are negative. This indicates that the densification was also influenced by the Laplace pressure, P_L, induced by the surface tension in pores formed by the powder particles besides the applied pressure, P, and the action of these pressures is additive. The Laplace pressure is 43.8 MPa for kinetics $\sqrt[4.5]{\dot{X}_{d(2)}(n=4.5,\rho)}$ and 35.3 MPa for $\sqrt[4]{\dot{X}_{d(3)}(n=4,\rho)}$.

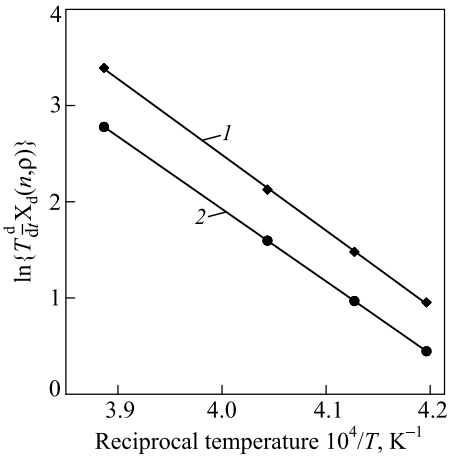

Fig. 3. Dependences $\ln\{T\dot{X}_{d(2)}(n=4.5,\rho)\}$ (*1*) and $\ln\{T\dot{X}_{d(3)}(n=4,\rho)\}$ (*2*) vs. reciprocal temperature T^{-1}

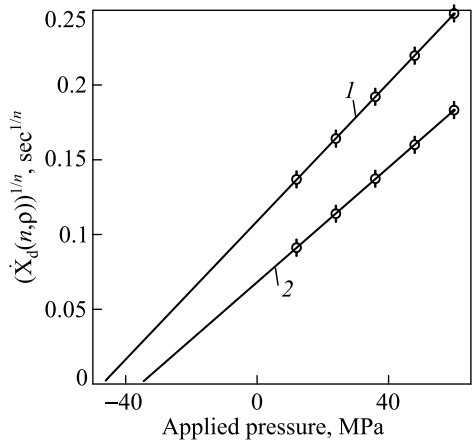

Fig. 4. Densification kinetics roots $\sqrt[4.5]{\dot{X}_{d(2)}(n=4.5,\rho)}$ (*1*) and $\sqrt[4]{\dot{X}_{d(3)}(n=4,\rho)}$ (*2*) vs. applied pressure

In the case of a powder material formed by irregular particles, the Laplace pressure is consistent with that for isothermal pressure sintering of tungsten and titanium carbides [11], when the estimated Laplace pressure for the sintering of TiC with regular particles of somewhat greater average size turned out to be higher than for the sintering of WC with irregular particles of somewhat smaller average size. The high Laplace pressure for the sintering of ZrB_2 found in this research confirms that the powder has an extensive internal surface because of fine particles.

NONISOTHERMAL PRESSURE SINTERING

Non-isothermal pressure sintering of ZrB_2 powder was carried out under conditions of constant rate of temperature $(\mathrm{d}/\mathrm{d}t)T =$ 20°C/min and $(\mathrm{d}/\mathrm{d}t)T =$ 40°C/min and a fixed external pressure of 48 MPa. Figure 5 shows typical dependences of the relative density ρ and temperature T in nonisothermal sintering of the ZrB_2 powder at an applied pressure of 48 MPa at heating rates of 20°C/min (*a*, *b*) and 40°C/min (*c*) versus sintering time.

According to above Eqs. (2) and (3), the densification of a porous body during sintering is accompanied by decrease in the root-mean-square stresses in the matrix and increase in the root-mean-square strain rate of the matrix. Respective data for the densification depicted in Fig. 5*a*, at $\varphi = \rho^{(2.5-\rho)/\rho}$ (*a*) and $\varphi = \rho^{(3.5-\rho)/\rho}$ (*b*), are presented in Fig. 6. When relative density $\rho \to 1$, the root-mean-square stress in the porous body matrix $\langle \tau_m \rangle \to 0$ and the root-mean-square strain rate $\langle \dot{\varepsilon}_m \rangle$ of the matrix changes along the curve, reaches its maximum, and then sharply decreases [18]. Although the dependences in Figs. 6*a* and 6*b* are generally similar, the root-mean-square stresses differ with the same initial data.

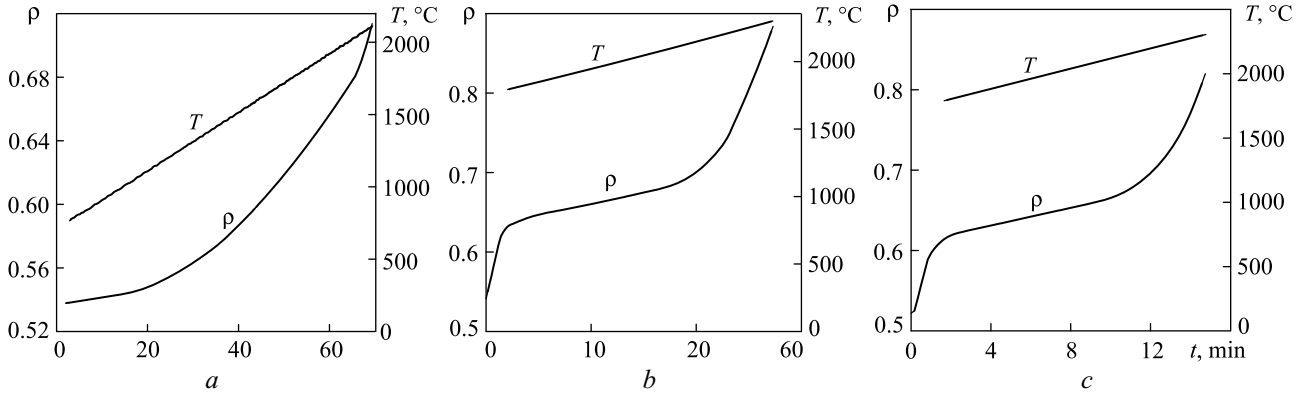

Fig. 5. Time dependences of the relative density ρ and temperature T in nonisothermal sintering of the ZrB_2 powder at an applied pressure of 48 MPa and heating rates of 20 (*a*, *b*) and 40°C/min (*c*)

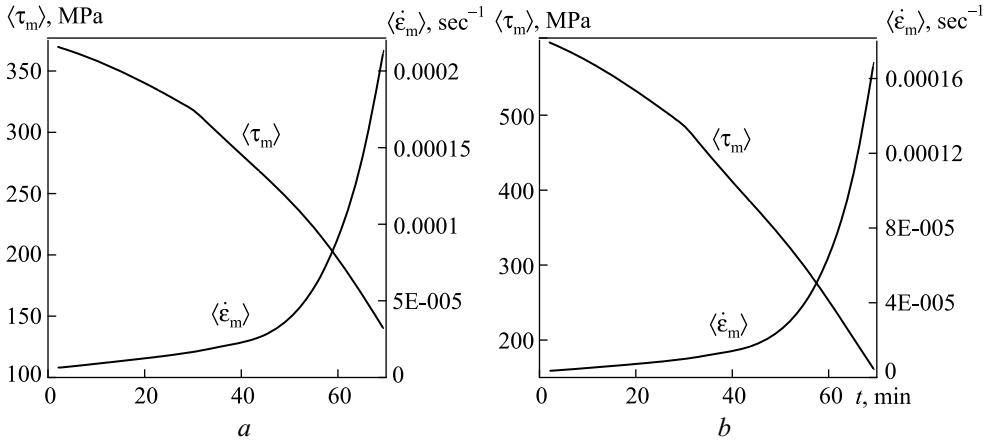

Fig. 6. Root-mean-square stress and strain rate for the porous body matrix vs. nonisothermal sintering time for ZrB_2 in accordance with data in Fig. 5*a*

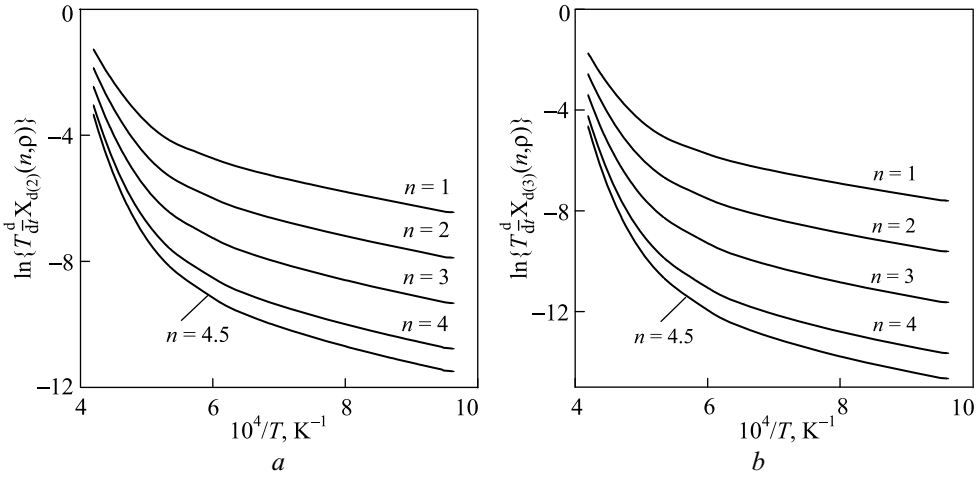

Fig. 7. Dependences $\ln\left\{T\dot{X}_{d(2)}(n,\rho)\right\}$ (*a*) and $\ln\left\{T\dot{X}_{d(3)}(n,\rho)\right\}$ (*b*) upon reciprocal thermodynamic temperature T^{-1} in accordance with data in Fig. 5*a*

Quantitative analysis of the kinetics of non-isothermal sintering in comparison with isothermal one is complicated by the temperature dependence of fluidity A in accordance with Eq. (6), which makes it impossible to use integrals (8a) or (8b). Therefore, the modeling of the densification kinetics was carried out using equations (7a) and (7b), containing the densification rate. It is known that integration smooths the experimental data and differentiation looses them. In order to reduce such a loosening, the tabulated experimental time dependences of the relative density were processed out by the method of approximation by power polynomials according to the criterion of the least squares [19] with automatic differentiation of the latter to give current values of the densification rate. Lagrange polynomials were also used, which do not require a fixed step of changing the argument. Since nonlinearity indicator *n* was not known in advance; it was varied in the approximation process.

Figure 7 presents dependences $\ln\left\{T\dot{X}_{d(2)}(n,\rho)\right\}$ and $\ln\left\{T\dot{X}_{d(3)}(n,\rho)\right\}$ vs. reciprocal thermodynamic temperature T^{-1} in accordance with Fig. 5*a*. These dependences turned out to be nonlinear, which indicates the temperature dependence of the activation energy.

Therefore, to calculate its current values by the approximation method, we first determined the change in the slope $\beta_{1(X)}$ of the above logarithms to the reciprocal temperature axis (Fig. 8). The reciprocal temperature

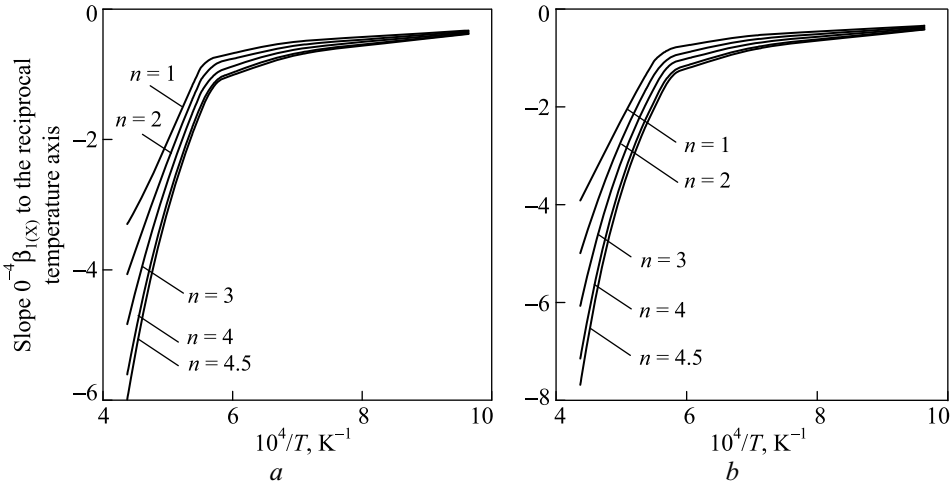

Fig. 8. Slope $\beta_{1(X)}$ of logarithms $\ln\left\{T\dot{X}_{d(2)}(n,\rho)\right\}$ (*a*) and $\ln\left\{T\dot{X}_{d(3)}(n,\rho)\right\}$ (*b*) to the reciprocal temperature axis in accordance with data in Fig. 5*a*

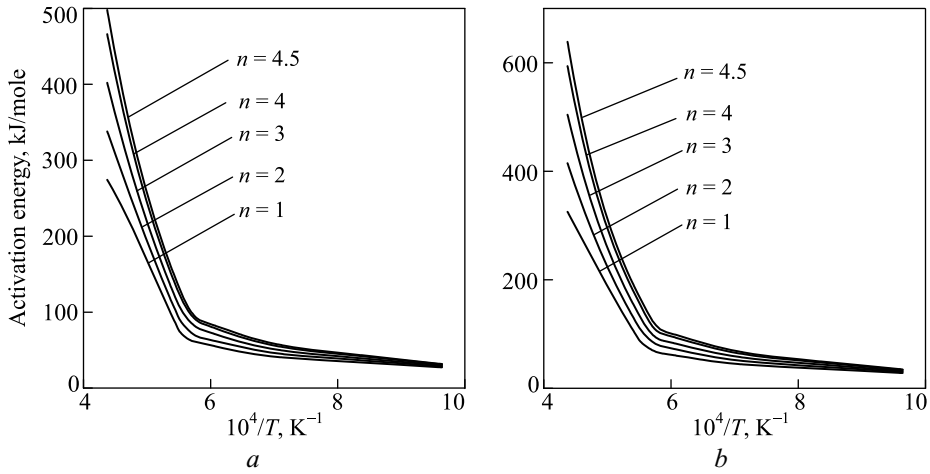

Fig. 9. Activation energy for ZrB_2 creep vs. reciprocal temperature at the conditionally low-temperature stage of nonisothermal pressure sintering in accordance with data in Fig. 8*a* and Fig. 8*b*

dependence of the activation energy at the conditionally low-temperature sintering stage (at 1545°C ≤ T ≤ 2015°C) is shown in Fig. 9. The lines change their slope sharply at 1345°C ≤ T ≤ 1545°C, indicating that ZrB_2 transforms from brittle to plastic condition. At temperatures from 765 to 1345°C, zirconium diboride is brittle and 1345°C can be accepted as its critical cold brittleness temperature.

At this sintering stage controlled by the thermally activated dislocation slip mechanism, the activation energy is known [20, 21] to depend on effective stresses in the materials induced by mechanical and thermal effects. At the selected heating rate, the contribution of thermal effect was insignificant. For this reason, the dependence of the activation energy on the root-mean-square stress was determined (Fig. 6). The results are illustrated in Fig. 10, showing only two straight sections that correspond to the linear dependence of the activation energy U on the root-mean-square stress $\langle \tau_m \rangle$ in the porous body matrix:

$$U = U_0 - v_a \langle \tau_m \rangle \tag{12}$$

(where v_a is the activation volume) at the conditionally low-temperature (to 2015°C) sintering stage. They are ascending line n = 3 in Fig. 10*a* and ascending line n = 2 in Fig. 10*b*. For line n = 3, U_0 = 868 kJ/mol and v_a =

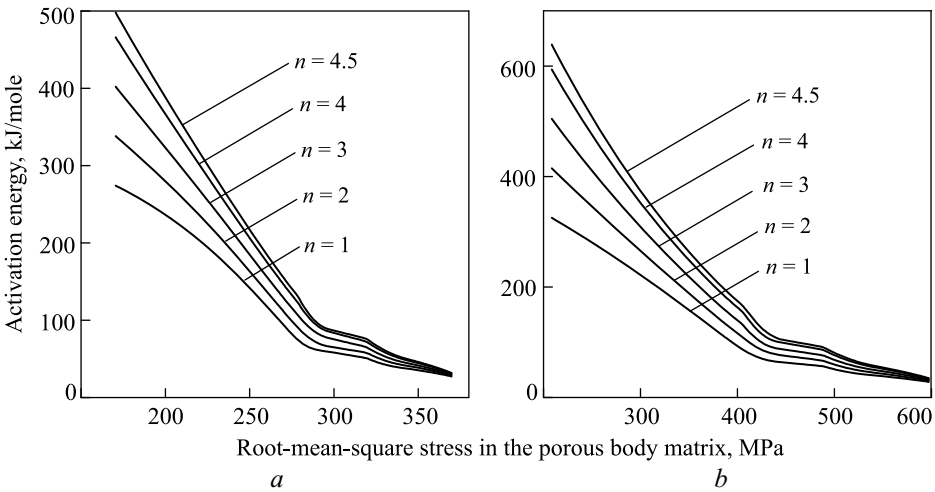

Fig. 10. Activation energy for ZrB_2 creep vs. the root-mean square stress at the conditionally low-temperature stage of nonisothermal pressure sintering in accordance with data in Fig. 9*a* and Fig. 9*b*

$= 2.735 \cdot 10^{-3}$ m^3/mol; for line $n = 2$, $U_0 = 730$ kJ/mol and $v_a = 1.615 \cdot 10^{-3}$ m^3/mol. Line $n = 4$ in Fig. 10*a* is also almost straight and is characterized by high $U_0 = 1032$ kJ/mol and $v_a = 3.318 \cdot 10^{-3}$ m^3/mol.

Comparing the activation energy and activation volume with viscous flow nonlinearity $n = 2$ that corresponds to the activated dislocation slip at a sufficient concentration of point defects, we can conclude that the densification kinetics at the conditionally low-temperature (to 2015°C) stage of nonisothermal pressure sintering of porous ZrB_2 is described by Eq. (7b) with $n = 2$.

The calculated logarithmic expressions for the densification kinetics of the ZrB_2 powder in nonisothermal pressure sintering versus time in a narrow temperature range and with a higher initial temperature (Figs. 5*b* and 5*c*) are provided in Figs. 11 and 12. The data show the same kinetics in pressure sintering at high temperatures depending on the rate of temperature increase. There are two clear temperature ranges where actually straight lines $\ln\left\{T\dot{\mathrm{X}}_{\mathrm{d}(2)}(n,\rho)\right\}$ and $\ln\left\{T\dot{\mathrm{X}}_{\mathrm{d}(3)}(n,\rho)\right\}$ have different slopes to the inverse temperature axis. The activation energies calculated from the slopes of these lines to the T^{-1} axis in accordance with Fig. 11 are provided in Table 1 and those in accordance with Fig. 12 in Table 2.

Low activation energies in ranges 1857°C ≤ T ≤ 2060°C and 1557°C ≤ T ≤ 1815°C at heating rates of 20 and 40°C/min, respectively, cannot be associated with the movement of vacancies. They could be attributed to the mobility of atoms but may emerge in the quantity sufficient to determine the viscous strain of a crystalline body only in exposure to radiation, which is absent in this case. Low activation energy may be shown only by a cooperative

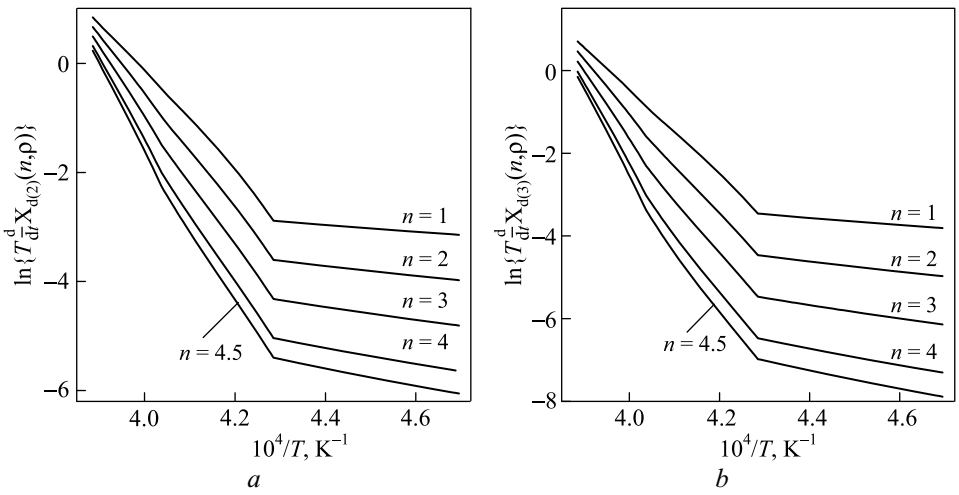

Fig. 11. Dependences $\ln\left\{T\dot{\mathrm{X}}_{\mathrm{d}(2)}(n,\rho)\right\}$ (*a*) and $\ln\left\{T\dot{\mathrm{X}}_{\mathrm{d}(3)}(n,\rho)\right\}$ (*b*) vs. reciprocal thermodynamic temperature T^{-1} in accordance with data in Fig. 5*b*

TABLE 1. Activation Energy (kJ/mol) for the Viscous Flow of the Porous ZrB_2 Matrix in Nonisothermal Sintering at an Applied Pressure of 48 MPa and a Heating Rate of 20°C/min

Flow nonlinearity exponent	Lines $\ln\left\{T\dot{\mathrm{X}}_{\mathrm{d}(2)}(n,\rho)\right\}$		Lines $\ln\left\{T\dot{\mathrm{X}}_{\mathrm{d}(3)}(n,\rho)\right\}$	
	1857°C ≤ T ≤ 2060°C	2061°C ≤ T ≤ 2301°C	1857°C ≤ T ≤ 2060°C	2061°C ≤ T ≤ 2301°C
$n = 1$	49	778	71	850
$n = 2$	74	883	106	964
$n = 3$	98	981	138	1028
$n = 4$	123	1050	171	1108
$n = 4.5$	134	1067	184	1144

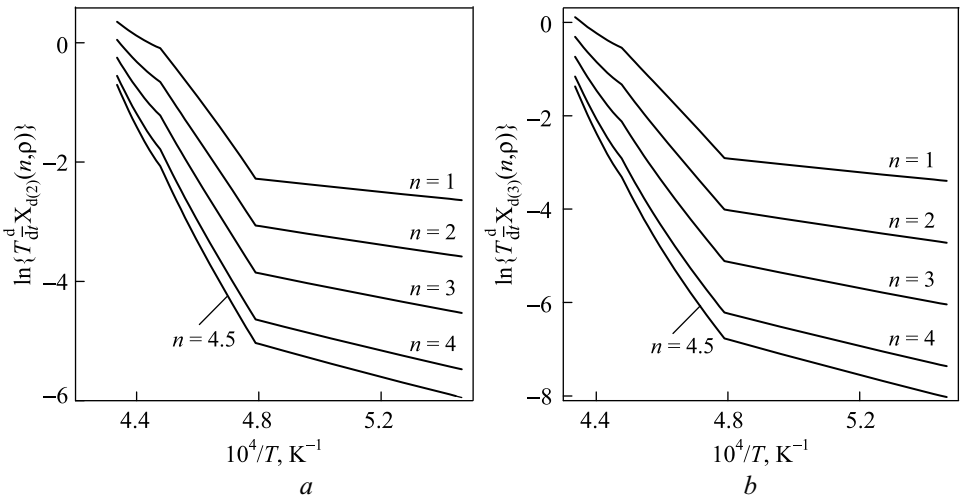

Fig. 12. Dependences $\ln\left\{T\dot{X}_{d(2)}(n,\rho)\right\}$ (*a*) and $\ln\left\{T\dot{X}_{d(3)}(n,\rho)\right\}$ (*b*) versus reciprocal thermodynamic temperature T^{-1} in accordance with data in Fig. 5*c*

TABLE 2. Activation Energy (kJ/mole) for the Viscous Flow of the Porous ZrB_2 Matrix in Nonisothermal Sintering at an Applied Pressure of 48 MPa and a Heating Rate of 40°C/min

Flow nonlinearity exponent	Lines $\ln\left\{T\dot{X}_{d(2)}(n,\rho)\right\}$		Lines $\ln\left\{T\dot{X}_{d(3)}(n,\rho)\right\}$	
	1557°C ≤ T ≤ 1815°C	1816°C ≤ T ≤ 2033°C	1557°C ≤ T ≤ 1815°C	1816°C ≤ T ≤ 2033°C
$n = 1$	44	483	60	503
$n = 2$	64	572	87	678
$n = 3$	83	661	114	803
$n = 4$	103	750	142	928
$n = 4.5$	113	794	155	990

process, causing deformation of a body with a large activation volume. That is, this is plastic deformation induced by the relaxation of thermal stresses in transition from accelerated initial heating to controlled slow heating.

The temperature range 2061°C ≤ T ≤ 2301°C (Table 1) practically corresponds to the temperature range in which the isothermal pressure sintering of zirconium diboride powder was carried out, so it is expedient to compare the data corresponding to the same values of the flow nonlinearity exponent n. This comparison indicates significantly higher values of the activation energy of the nonlinear viscous flow of zirconium diboride in non-isothermal pressure sintering. It is known that an increase in the activation energy in chemical reactions controlled by a diffusion mechanism characterizes the endothermic process, and a decrease in the activation energy indicates an exothermic process. A striking example is the oxidation of metals, which is exothermic, i.e. accompanied by the release of heat, but the inverse process of reduction of metals from oxides is endothermic (accompanied by heat absorption). The thermal effects of phase transformations are determined by changes in the heat capacity. An exothermic effect occurs in transition from higher heat capacity to lower heat capacity. The inverse transition to higher heat capacity is accompanied by an endothermic effect.

Experimental results for pressure sintering with controlled heating show that it is endothermic because increasing temperature leads to greater heat capacity. Somewhat lower activation energies in the range 1816°C ≤ ≤ T ≤ 2033°C for nonisothermal sintering at a heating rate of 40°C/min imply that the energy absorption effect increases with temperature, being predominant over the heating rate.

CONCLUSIONS

According to the results of an experimental study on the densification of zirconium diboride powder during the sintering under external pressure from 12 to 60 MPa in vacuum in conditions of isothermal exposure at temperatures in the range of 2110–2300°C, a quantitative analysis of densification kinetics was carried out within the framework of continuum theory for bulk viscous flow of porous body taking into account the influence of the shape of the powder particles on the rheological properties of the porous body.

It is established that this kinetics is described by the equation of the steady-state nonlinear creep of the matrix, which forms a porous body, with the root-mean-square strain rate of the viscous flow proportional to the fourth exponent of the root-mean-square stress. The root-mean-square strain rate decreases over time much faster than the root-mean-square stress. Both quantities tend to zero in approaching the nonporous state of the sinterable material.

The estimated activation energy taking into account the irregular shape of the powder particles is 626 kJ/mol. The obtained value indicates that the creep of the matrix of the porous body is controlled by the dislocation climb mechanism with activation energy that is consistent with the self-diffusion of atoms in the metallic sublattice of zirconium diboride.

The estimated value of the Laplace pressure generated by the surface tension of the ensemble of zirconium diboride powder particles is 35.3 MPa. This value practically does not yield to the average value of the selected external pressures and is indicative of extensive surface of the powder material.

The pressure sintering in the non-isothermal mode of controlled heating with constant rates of temperature increase of 20 and 40°C/min is characterized by the curve of increasing the root-mean-square strain rate with a maximum. After passing through the maximum a strain rate sharply slows.

The study of pressure sintering kinetics during the non-isothermal mode showed the presence of two temperature ranges with different values of activation energy. Sintering with a controlled heating rate from 765°C revealed the transition of the brittle state of zirconium diboride at a temperature of 1345°C to plastic one and the beginning of a nonlinear viscous flow of the porous body matrix at 1545°C.

In the temperature range from 1545 to 2015°C, the root-mean-square creep rate of a porous body matrix is proportional to the square of the root mean square stress and is characterized by a linear dependence of the activation energy on it with a proportionality coefficient, which is the activation volume. Its estimated value is $1.615 \cdot 10^{-3}$ m^3/mol. The activation energy decreases linearly from 730 kJ/mol. These data indicate that the creep of the matrix of the porous body is controlled by the mechanism of thermally activated sliding dislocations.

In narrower temperature intervals with a higher initial temperature of non-isothermal sintering, the densification kinetics is characterized by activation energy values that significantly exceed the corresponding data for isothermal sintering. This indicates the endothermic nature of the non-isothermal pressure sintering mode of zirconium diboride.

REFERENCES

1. F. Monteverde, D.D. Fabbriche, and A. Bellosi, “Zirconium diboride-based composites,” *Key Eng. Mater.*, **206–213**, 961–964 (2002).
2. J.J. Meléndez-Martínez, A. Domínguez-Rodríguez, F. Monteverde, C. Melandri, and G. Portu, “Characterization and high temperature mechanical properties of zirconium boride-based materials,” *J. Eur. Ceram. Soc.*, **22**, Issues 14–15, 2543–2549 (2002).
3. A.L. Chamberlain, W.G. Fahrenholtz, and G.E. Hilmas, “Low-temperature densification of zirconium diboride ceramics by reactive hot pressing,” *J. Am. Ceram. Soc.*, **89**, Issue 12, 3638–3645 (2006).
4. J.K. Sonber, T.S.R.Ch. Murthy, C. Subramanian, Kumar Sunil, R.K. Fotedar, and A.K. Suri, “Investigations on synthesis of ZrB_2 and development of new composites with HfB_2 and $TiSi_2$,” *Int. J. Refract. Met. Hard Mater.*, **29**, 21–30 (2011).
5. M.J. Thompson, Densification and Thermal Properties of Zirconium Diboride Based Ceramics, Doctoral Dissertations, p. 2150; https://scholarsmine.mst.edu/doctoral_dissertations/2150. 2012.

6. E.W. Neuman, Elevated Temperature Mechanical Properties of Zirconium Diboride Based Ceramics, Doctoral Dissertations, p. 2164; http://scholarsmine.mst.edu/doctoral_dissertations/2164. 2014.
7. M.W. Bird, R.P. Aune, A.F. Thomas, P.F. Becher, and K.W. White, "Temperature-dependent mechanical and long crack behavior of zirconium diboride–silicon carbide composite," *J. Eur. Ceram. Soc.*, **32**, 3453–3462 (2012).
8. O.N. Grigoriev, V.B. Vinokurov, L.I. Klimenko, N.D. Bega, and N.I. Danilenko, "Sintering of zirconium diboride and phase transformations in the presence of Cr_3C_2," *Powder Metall. Met. Ceram.*, **55**, No. 3–4, 185–194 (2016).
9. S. Chakraborty, P.K. Das, and D. Ghosh, "Spark plasma sintering and structural properties of ZrB_2 based ceramics: a review," *Rev. Adv. Mater. Sci*., **44**, 182–193 (2016).
10. V.B. Vinokurov, M.S. Kovalchenko, L.I. Klimenko, N.D. Bega, and T.V. Mosina, "Kinetics of nonisothermal pressure sintering of zirconium diboride powder with additives of boron and chromium carbides in vacuum," *Powder Metall. Met. Ceram.*, **57**, No. 1–2, 27–37 (2018).
11. M.S. Kovalchenko, "Pressure sintering kinetics of tungsten and titanium carbides," *Int. J. Refract. Met. Hard Mater*., **39**, 32–37 (2013).
12. V.V. Skorokhod, *Rheological Fundamentals of Sintering Theory* [in Russian], Naukova Dumka, Kyiv (1972), p. 151.
13. M.S. Kovalchenko, "Pressure sintering of powder materials," *Powder Metall. Met. Ceram.*," **50**, No. 1–2, 18–33 (2011).
14. M.S. Kovalchenko, "Rheological models of pressure sintering of powders," *Powder Metall. Met. Ceram.*, **52**, No. 1–2, 7–19 (2013).
15. M.S. Kovalchenko, "Rheology and kinetics of pressure sintering," *Mater. Sci. Forum*, **835**, 76–105 (2016).
16. M.S. Kovalchenko, T.P. Hrebenok, N.P. Brodnikovskii, and A.A. Rogozinskaya, "Features of brittle material powder compaction during pressing," *Powder Metall. Met. Ceram.*, **55**, No. 5–6, 259–269 (2016).
17. D.S. Wilkinson and M.F. Ashby, "Pressure sintering by power law creep," *Acta Met.*, **23**, 1277–1285 (1975).
18. T.P. Hrebenok, V.I. Subbotin, and M.S. Kovalchenko, "Densification kinetics of titanium carbide based cermet during the pressure sintering," *Aspects Min. Miner. Sci.*, **4**, Issue 4, 517–518 (2020).
19. A. Angot, *Mathematics for Electrical and Telecommunications Engineers* [in French], Éditions de la Revue d'Optique, Paris (1949), p. 660.
20. J. Friedel, *Dislocations*, Pergamon Press, Oxford–London–Edinburgh–New York–Paris–Frankfurt (1964), p. 512.
21. G.P. Cherepanov, "Chapter 4. Physics of sintering," in: *Solid Mechanics and Its Applications, Vol. 51: Methods of Fracture Mechanics: Solid Matter Physics*, Kluwer Academic Publishers, Dordrecht (1997), p. 333.